Int. J. Electrochem. Sci., 11 **(2016)** 8633 – 8645, doi: 10.20964/2016.10.01

International Journal of
ELECTROCHEMICAL
SCIENCE
www.electrochemsci.org

Synthesis and Electrocatalytic Properties of $La_{1-x}Sr_xCoO_3$ ($0 \leq x \leq 0.8$) Film Electrodes for Oxygen Evolution in Alkaline Solutions

Manish Kumar Yadav, Ritu Yadav, Priya Sharma and N. K. Singh[*]

Department of Chemistry, Faculty of Science, University of Lucknow, Lucknow-226007 INDIA
[*]E-mail: nksbhu@yahoo.com, singh_narendra@lkouniv.ac.in

Received: 9 June 2016 / *Accepted:* 22 July 2016 / *Published:* 6 September 2016

Perovskite-type oxides of lanthanum and cobalt with composition $La_{1-x}Sr_xCoO_3$ (x = 0.0, 0.2, 0.4, 0.6 and 0.8) have been prepared by a low temperature sol-gel route. Electrodes of the material were formed on pretreated Ni-support by oxide slurry painting technique and studied their electrochemical behavior with regards to oxygen evolution reaction (OER) in aqueous KOH solution. The electrochemical characterization was done in three electrode single compartment glass cell using Gamry (Reference 600) Electrochemical Work Station. Techniques used for electrochemical studies were cyclic voltammetry and Tafel polarization. The data showed that the substitution of Sr (0.2 - 0.8 mol) increased the electrocatalytic activity of the oxide. The value was found to be highest with 0.8 mol Sr. The Tafel slopes and reaction order with respect to OH^- concentration for oxygen evolution reaction were found to be 65-77 $mVdecade^{-1}$ and unity, respectively. The cyclic voltammogram recorded between 0.0 – 0.7 V in 1M KOH at 25^0C exhibited a pair of redox peaks prior to oxygen evolution reaction. The thermodynamic parameters for oxygen evolution reaction such as, standard electrochemical enthalpy of activation ($\Delta H_{el}^{0\#}$), standard enthalpy of activation ($\Delta H^{0\#}$), and standard entropy of activation ($\Delta S^{0\#}$) have also been calculated by recording the Tafel polarization curve in 1 M KOH at different temperatures. Oxide samples were characterized physicochemically by scanning electron microscope (SEM) powder X-ray diffraction (XRD) techniques.

Keywords: Perovskite-type oxide, sol-gel, XRD, Electrolcatalysis, Thermodynamic parameters

1. INTRODUCTION

The perovskite-type oxides having general formula ABO_3, where, A is the cation of large size (like La, Sm) and B is transition metal ions, are known to be important electrocatalysts [1-5] and well investigated for water electrolysis, fuel cells, auto-exhaust treatment etc. In the past, these materials were prepared by conventional ceramic and thrmal decomposition methods [6-11], which required very high temperature and produced oxides with high particle size and low specific surface area. Oxides

obtained by these methods also showed very low electrocatalytic activity. However, oxides produced by suitable low temperature procedure have smaller particle size with high specific surface area.

During the last few decades, some low temperature synthetic routes with suitable precursors have been reported in literature [12-16]. These methods involve the use of amorphous organic acid, like malic, citric, steric, polyacrylic acid etc, hydroxide and solid solutions, and binuclear complexes of compartmental ligands. By adopting these low methods, Singh et al. [17-28] prepared a series of perovskite-type oxides; $LaCoO_3$, $LaMnO_3$, $LaNiO_3$ with their substituted derivatives and studied their electrocatalytic properties for OER in alkaline solutions. The electrocatalytic activity of these materials was observed to be much better than previously prepared by conventional ceramic and high temperature thermal decomposition methods. Recent literature [29-42] showed that the electrocatalytic properties of pure, composite and bifunctional perovskite oxides have been studied by number of researchers with regards to oxygen evolution reaction (OER) as well as oxygen reduction reaction (ORR).

In 1998, Singh et al [25] reported the electrocatalytic properties of strontium substituted lanthanum manganites obtained by citric acid-ethylene glycol precursor route [16]. By adopting the similar method [16, 25], we produced mixed oxides of La, Sr and Co in the form of oxide film electrode. The electrodes were further used to study the ectrocatalytic properties with regards to OER. Details of results are described here.

2. EXPERIMENTAL

Mixed oxides $La_{1-x}Sr_xCoO_3$ (x = 0.0, 0.2, 0.4, 0.6 and 0.8) were prepared by low temperature sol-gel route as reported by Vassiliou et al. [16]. All the chemicals and reagents used in each preparation were of analytical grade and purified. In the process of synthesis, weighed amount of $La(NO_3)_3.6H_2O$ (Merck 99%), $Sr(NO_3)_2$ (Merck, 99%) and $Co(NO_3)_2.6H_2O$ (Merck, 97%) were dissolved in 100 ml double distilled water as per stoichiometric ratio of the oxide. In this an excess quantity of citric acid (Merck, purified), few ml of ethylene glycol (Merck, 96%) and 2 drops of HNO_3 (Merck) were added with constant stirring. The solution was then evaporated on water bath. The gel formed after evaporation was heated gradually to decompose on the hot plate. The material, so obtained, was crushed into agate pastel mortar to get the fine powder, which was finally sintered at 650 °C for 5 hr in a PID controlled electrical furnace to obtain the desired oxide. During each preparation, the ratio of metal ions, citric acid and ethylene glycol was kept constant to 4 g: 10 g: 4 ml, respectively.

The oxide, so prepared, was confirmed for its perovskite phase by recording X-ray diffraction pattern (XRD) using XPERT-PRO Diffractometer (Model PW3050/60; Radiation Source: Cu-Kα; λ = 1.54048 Å). The texture morphology of the oxide powder sintered at 650 °C for 5 hr was examined by scanning electron microscope (JOEL JSM 6490LV). In order to get the electrochemical studies, oxide powders were transformed into the oxide film electrodes on Ni-support. For the purpose, slurry of the oxide powder with Triton X-100 was prepared, painted on to one side of the pre-treated Ni-support and subsequently heat treated at 380 °C for 1½ hr. The coating of the slurry was repeated 2-3 timed to obtain the desired loading on the conducting support. The electrical contact with the oxide film was

made by using copper wire, silver paste and Araldite epoxy. The treatment of Ni-support and electrical connection with the oxide film to form the oxide film electrode were done in the same way as described earlier [17, 22]. The electrocatalytic properties of the material were studied in a three electrode single compartment glass cell using cyclic voltammetry (CV) and Tafel polarization techniques. For the purpose, an electrochemical work station (Gamry Reference 600 ZRA) having potentiostat/galvanostat provided with corrosion and physical electrochemistry software and a desktop computer (HP) was used. A platinum foil (~2 cm^2) and Hg/HgO/1M KOH (E° = 0.098 V vs NHE at 25°C) were used as an auxiliary and reference electrodes, respectively. In order to get the minimum solution resistance (iR drop) between the working and reference electrode, a Luggin capillary (agar-agar and potassium chloride gel) was employed to make the connection between them. The oxide film electrode was used as working electrode. The formal overpotential values mentioned in the data were obtained by the relation, $\eta = E - E_{O_2/OH^-}$, where E and E_{O_2/OH^-} (= 0.303 V vs. Hg/HgO) [43] are the applied potential across the catalyst/ 1 M KOH interface and the theoretical equilibrium Nernst potential in 1 M KOH at 25 °C, respectively.

3. RESULT AND DISCUSSION

3.1 Physicochemical Properties

3.1.1 Scanning Electron Micrograph (SEM)

a 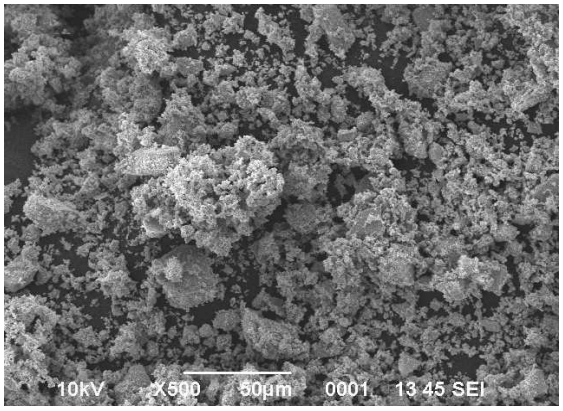

$LaCoO_3$

b 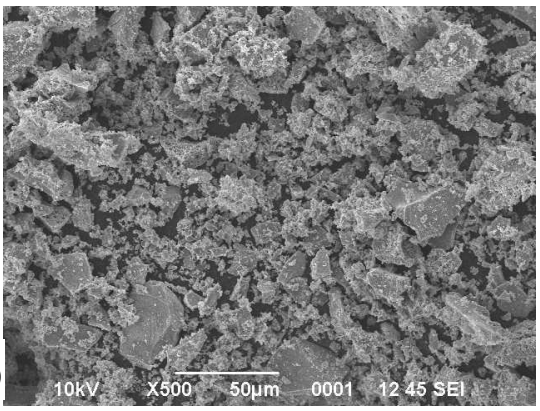

$La_{0.8}Sr_{0.2}CoO_3$

c 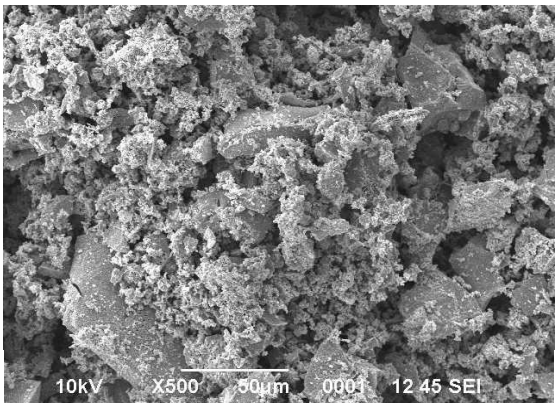

$La_{0.6}Sr_{0.4}CoO_3$

d 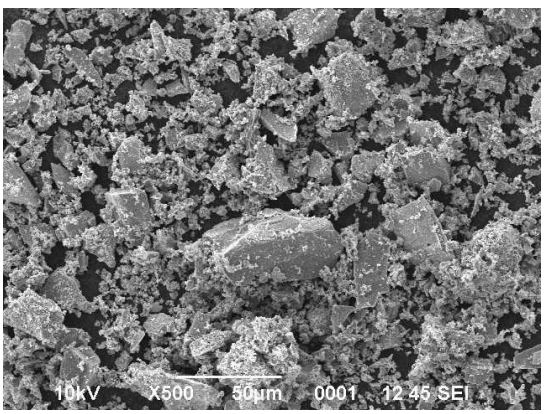

$La_{0.4}Sr_{0.6}CoO_3$

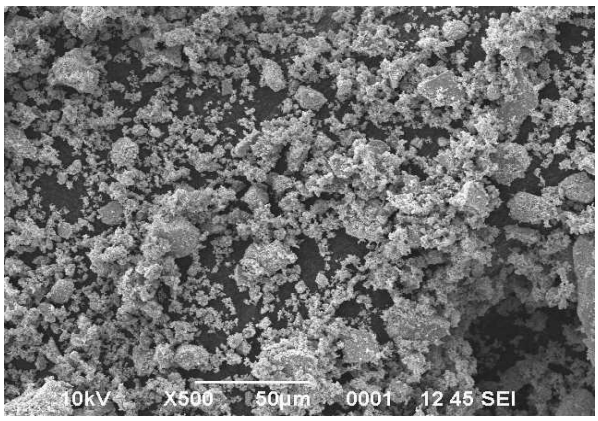

Figure 1. SE-micrograph of the oxide powder sintered at 650°C for 5 hrs. a: $LaCoO_3$, b: $La_{0.8}Sr_{0.2}CoO_3$, c: $La_{0.6}Sr_{0.4}CoO_3$ d: $La_{0.4}Sr_{0.6}CoO_3$ e: $La_{0.2}Sr_{0.8}CoO_3$

SE-micrograph of the each oxide has been carried out in the form fine powder and the results, so obtained, are shown in Fig. 1 (A-D) at magnification ×500. Figure indicates that feature of each oxide powder is more or less similar in nature and grains do not follow definite structure. However, particle size of the material is influenced by Sr-substitution and found to be minimum with 0.8 mol Sr.

3.1.2 X-Ray Diffraction (XRD)

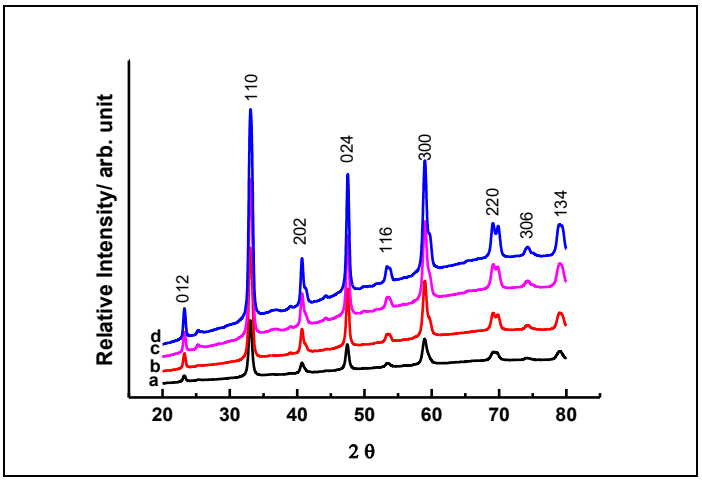

Figure 2. X-ray diffraction of oxide powder sintered at 650°C for 5 hrs. a: $LaCoO_3$, b: $La_{0.8}Sr_{0.2}CoO_3$, c: $La_{0.6}Sr_{0.4}CoO_3$ d: $La_{0.2}Sr_{0.8}CoO_3$

Powder X-ray diffraction pattern of the material sintered at 650 °C for 5 hr is recorded between 2θ = 20° and 80° and represented in Fig. 2. The data, so obtained, were analysed by using JCPDS-ICDD 1997 with reference no. 25-1060 and 36-1393 for $LaCoO_3$ and Sr-substituted products, respectively which indicates more or less hexagonal crystal geometry of the material with a = 5.434±0.007 Å and c = 13.153±0.065 Å. Values of crystallite size as estimated by using Scherer's formula [44] were found to be 28, 17 and 14 nm for $LaCoO_3$ & $La_{0.8}Sr_{0.2}CoO_3$, $La_{0.6}Sr_{0.4}CoO_3$ and $La_{0.2}Sr_{0.8}CoO_3$, respectively.

3.2. Electrochemical properties

3.2.1. Cyclic Voltammetry (CV)

The cyclic voltammogram of each oxide film electrode on Ni substrate was recorded at the scan rate 20 mV sec^{-1} in the potential region 0.0-0.7 V in 1M KOH at 25 ˚C. A representative curve for each oxide is shown in Fig. 3.

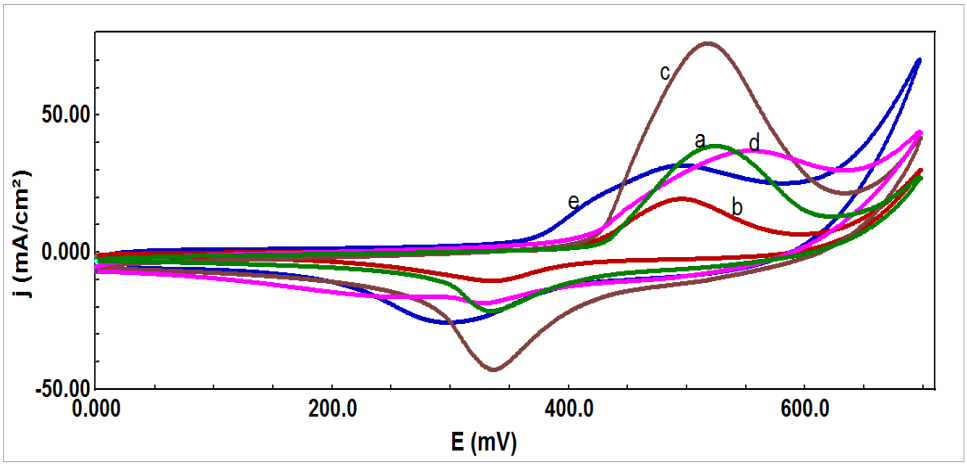

Figure 3. Cyclic voltammogram of $La_{1-x}Sr_xCoO_3$ ($0 \leq x \leq 0.8$) film electrode on Ni in 1M KOH at 25°C (scan rate = 20 mV sec^{-1}). a: $LaCoO_3$, b: $La_{0.8}Sr_{0.2}CoO_3$, c: $La_{0.6}Sr_{0.4}CoO_3$, d: $La_{0.4}Sr_{0.6}CoO_3$, e: $La_{0.2}Sr_{0.8}CoO_3$

Values of cyclic voltammetric parameters such as anodic (E_{Pa}) and cathodic (E_{Pc}) peak potentials, the peak separation potential ($\Delta E_p = E_{Pa}-E_{Pc}$), anodic and cathodic peak current (j_{p_a} & j_{p_c}) and the formal redox potential [$E^{\circ} = (E_{Pa}+E_{Pc})/2$] have been estimated from the CV curves and given in the Table 1. The table 1 and figure 3 showed that voltammograms of the oxide electrode exhibited a pair of redox peaks, one anodic (E_{Pa} = 524±30 mV) and a corresponding cathodic peak (E_{Pc} = 316±20 mV), prior to the onset of oxygen evolution reaction. Similar redox peaks have also been observed for $La_{1-x}Sr_xCoO_3$ film electrodes on Ni obtained by malic acid aided [17] and polyacrylic acid [22] ($E_{Pa} \approx$ 500 mV and $E_{Pc} \approx$ 310 mV at 20 mV sec^{-1}) methods in 1M KOH at 25 ˚C and for $La_{0.8}Sr_{0.2}Ni_{0.2}Co_{0.8}O_3$ ($E_{Pa} \approx$ 490 mV and $E_{Pc} \approx$ 350 mV at 30 mV sec^{-1}) [22, 45] in 30 wt% KOH. The cyclic voltammogram of the bare Ni [46] ($E_{Pa} \approx$ 490 mV and $E_{Pc} \approx$ 380 mV) in 1 M KOH indicates that the redox peaks observed in the present investigation result from the Ni substrate which might come in contact with the electrolyte during cycling process. Also, it is reported [1, 47] that oxides prepared at low temperature undergoes hydration easily in solution. The electrolyte may also penetrate the oxide film through pores, cracks and grain boundaries.

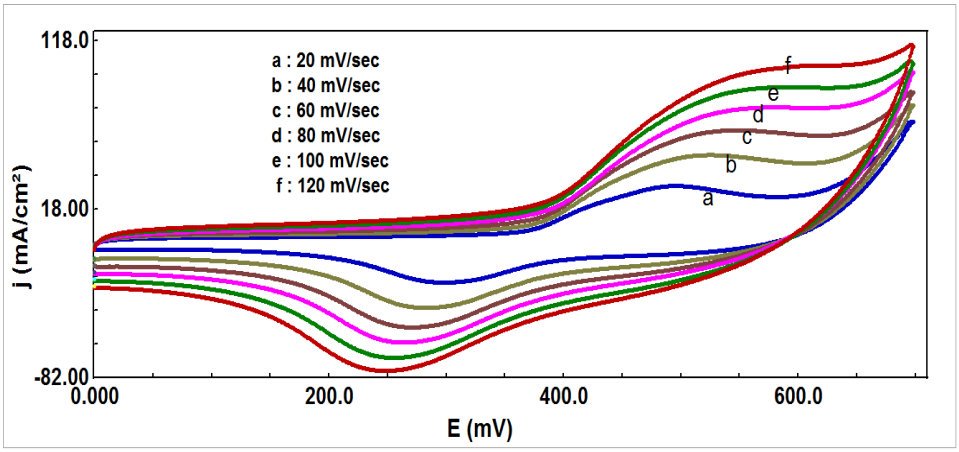

Figure 4. Cyclic voltammogram of the $La_{0.2}Sr_{0.8}CoO_3$ film on Ni at different scan rates in 1M KOH (25°C).

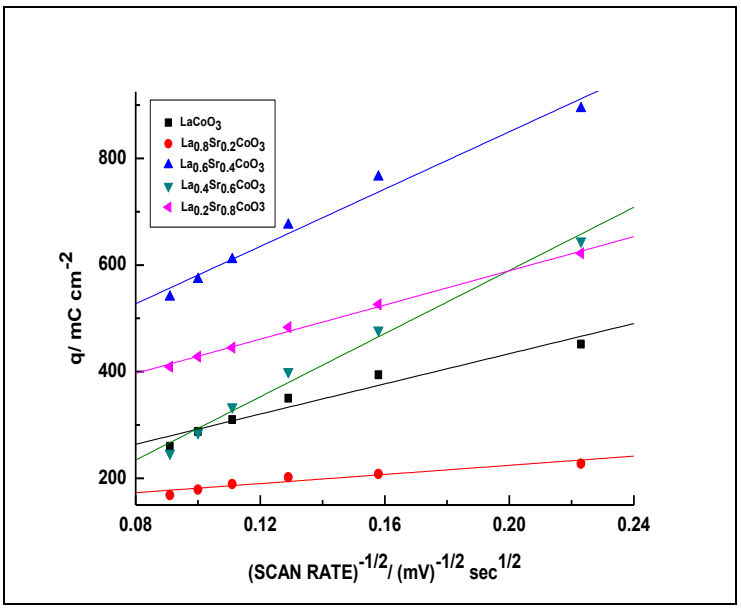

Figure 5. Plot of charge (q) vs (scan rate)$^{-1/2}$ for the oxide electrode $La_{1-x}Sr_xCoO_3$ ($0 \leq x \leq 0.8$) in 1 M KOH

To examine the influence of scan rates on the cyclic voltammetric parameters, CV curves were recorded at different scan rates ranging from 20 to 120 mV s^{-1} by keeping the experimental conditions similar. A representative voltammogram for $La_{0.2}Sr_{0.8}CoO_3$ is shown in Fig. 4. From figure it is observed that both anodic and cathodic peaks shifted either side as the scan rate is increased from 20 to 120 mV sec^{-1}. This indicates that the redox process is quasireversible. The voltammetric charge (q) was estimated by integrating the CV curve from zero to a potential just prior to the onset of oxygen evolution reaction. The linearity found in the plot of q vs (scan rate)$^{-1/2}$ (Fig. 5) indicates that the surface redox process is diffusion controlled.

Table 1. Cyclic Voltammetric parameters for $La_{1-x}Sr_xCoO_3$ ($0 \leq x \leq 0.8$) film electrodes at scan rate 20 mV sec^{-1} in 1M KOH at 25°C

Electrode	Ep_a /mV	Ep_c /mV	$\Delta E = Ep_a - Ep_c$ /mV	$E° = (E_{Pa} + E_{Pc})/2$ /mV	j_{p_a} /mA cm^{-2}	j_{p_c} /mA cm^{-2}	$\frac{j_{p_a}}{j_{p_c}}$
$LaCoO_3$	524	333	191	429	38.8	21.5	1.8
$La_{0.8}Sr_{0.2}CoO_3$	495	335	160	415	19.4	10.5	1.9
$La_{0.6}Sr_{0.4}CoO_3$	517	336	181	427	76.1	42.8	1.8
$La_{0.4}Sr_{0.6}CoO_3$	554	326	228	440	37.0	18.6	1.9
$La_{0.2}Sr_{0.8}CoO_3$	495	297	198	396	31.7	25.6	1.2

3.2.2. Double layer capacitance/Roughness factor

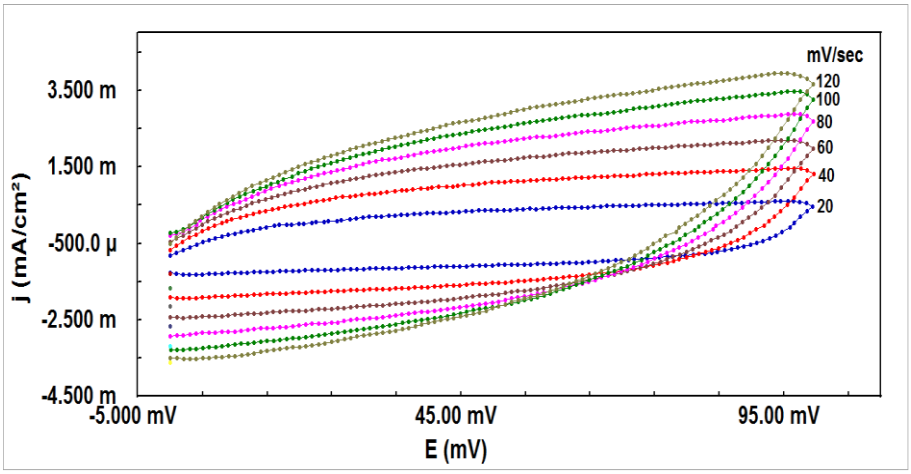

Figure 6. Typical CV curve for the Ni/$La_{0.4}Sr_{0.6}CoO_3$ electrode in the potential region 0.0-0.1V in 1M KOH at 25°C.

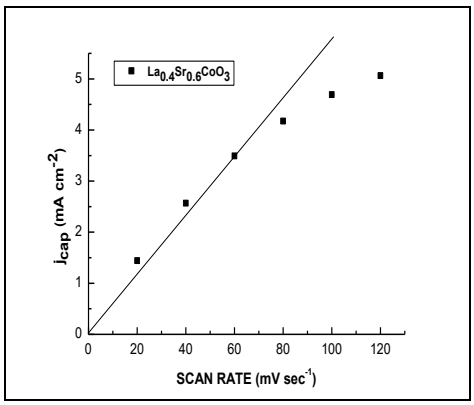

Figure 7. Plot of j_{cap} vs scan rate for the Ni/ $La_{0.4}Sr_{0.6}CoO_3$ electrode in 1M KOH at 25°C.

The roughness factor is determined only for the oxide electrode, $La_{0.4}Sr_{0.6}CoO_3$, since cyclic voltammetric curve for other materials was unsymmetrical in the small potential capacitive region (0.0-0.1 V). The value of capacitance double layer (C_{dl}) and its roughness factor was estimated by the method reported in literature [48]. The CV curve and its corresponding j_{cap} vs scan rate are represented

in Fig.6 and Fig. 7, respectively. The slope of the straight line obtained from j_{cap} vs scan rate plot gives the value of capacitance double layer. The corresponding roughness factor was estimated by assuming capacitance double layer of the smooth oxide surface, 60 μF cm^{-2} and the value of roughness factor was found to be 923 for the oxide electrode $La_{0.4}Sr_{0.6}CoO_3$.

3.2.3. Electrocatalytic activity

The electrocatalytic property of each oxide electrode was determined by recording the iR-uncompansated anodic polarization curve (*E* vs log *j*) in 1 M KOH at 25 ˚C at the scan rate of 0.2 mV s^{-1}. The anodic polarization curves, so obtained with each oxide electrode are shown in Fig. 8.

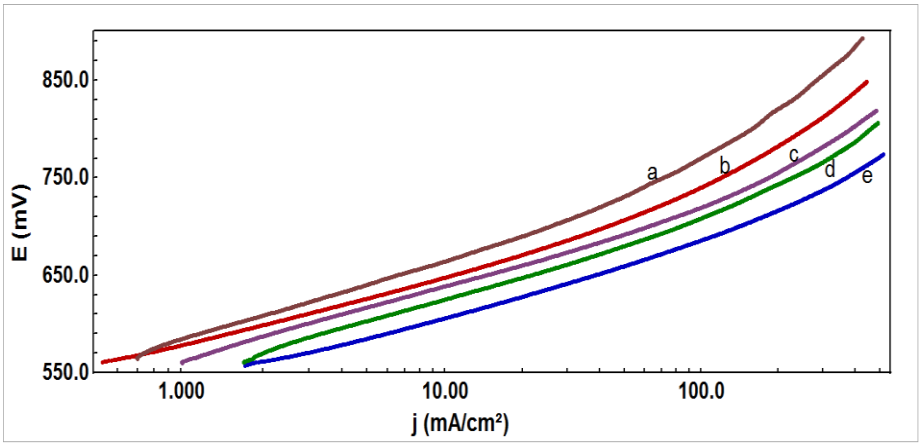

Figure 8. Tafel plots for the pure and Sr-substituted oxide film electrode on Ni in 1M KOH at 25°C; scan rate: 0.2mVsec^{-1}. a: $LaCoO_3$, b: $La_{0.8}Sr_{0.2}CoO_3$, c: $La_{0.6}Sr_{0.4}CoO_3$, d: $La_{0.4}Sr_{0.6}CoO_3$, e: $La_{0.2}Sr_{0.8}CoO_3$.

The polarization curves are found to be similar in nature and have two Tafel slope region; one at low potential and other at higher potential. These polarization curves are used to estimate the values of Tafel slope and electrocatalytic activity of the material. The electrocatalytic activity is determined in terms of current density at two different overpotentials as well as in terms of overpotential at two fixed current density and represented in Table 2. Values of Tafel slope were ranged between 66-77 mV decade^{-1}. Almost similar Tafel slope value was observed in the case of La and Co mixed perovskite-type oxides reported in literature [6-9,17]. From table 2, it is evident that the substitution of Sr for La in $LaCoO_3$ increased the electrocatalytic activity and the value was found to be maximum with 0.8 mol Sr-substitution. At overpotential 350 mV the catalytic activity of $La_{0.2}Sr_{0.8}CoO_3$ was observed to be ~ 6 times higher than that of base oxide. Based on the apparent current density data at a certain overpotential (η_{O_2} = 400 mV) the electrocatalytic activity of oxides followed the order:

$La_{0.2}Sr_{0.8}CoO_3$ (j_a = 151.9 mA cm^{-2}) > $La_{0.4}Sr_{0.6}CoO_3$ (j_a = 90.1 mA cm^{-2}) > $La_{0.6}Sr_{0.4}CoO_3$ (j_a =67.7mA cm^{-2}) > $La_{0.8}Sr_{0.2}CoO_3$ (j_a = 46.7 mA cm^{-2}) > $LaCoO_3$(j_a = 28.0 mA cm^{-2})

Similar trends of electrocatalytic activity have also been observed in terms of overpotential at a fixed current density.

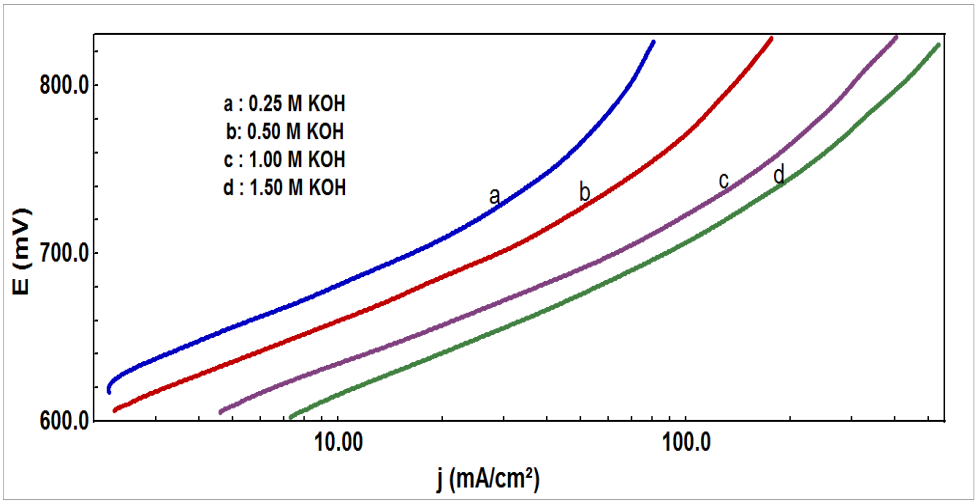

Figure 9. Tafel plots for oxygen evolution on the $La_{0.2}Sr_{0.8}CoO_3$ film on Ni at varying KOH concentrations (μ = 1.5) at 25°C.

In order to obtain the reaction order (*p*), the anodic polarization curve was recorded in different KOH concentration (Fig. 9). The ionic strength of the electrolyte at each concentration was kept constant (μ =1.5) by using KNO_3 (Merck 98%) as an inert electrolyte.

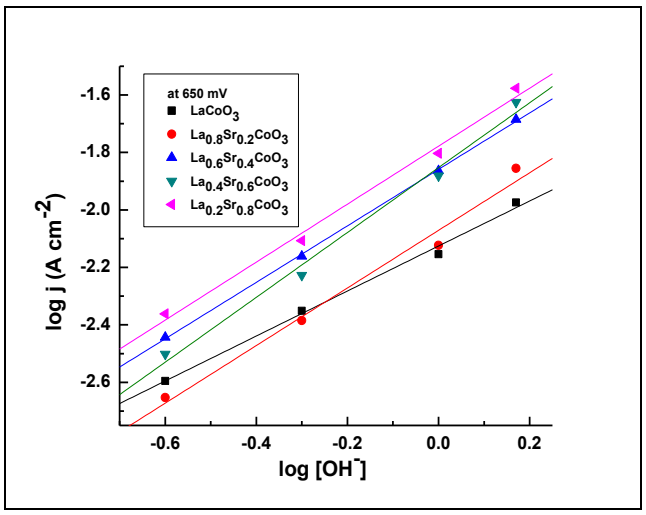

Figure 10. Plot of log j vs. log [OH^-] for $La_{1-x}Sr_xCoO_3$ ($0 \leq x \leq 0.8$) film electrode on Ni at 25°C at a constant applied potential (E = 650 mV).

The order of reaction was estimated from the slope of the straight line plot log *j* vs log [OH^-] (Fig. 10) at a fixed potential (*E* = 650 mV). The value of reaction order was found to be unity with each oxide electrode and given in Table 2. The first Tafel region of the polarization curve, obtained at different KOH concentrations, was generally considered to take the current density value. The observed values of reaction order and Tafel slope suggest that each oxide electrode follows more or less same mechanistic paths for the oxygen evolution reaction.

Table 2. Electrode kinetic parameters for oxygen evolution on Ni/$La_{1-x}Sr_xCoO_3$ ($0 \leq x \leq 0.8$) film electrodes in 1M KOH at 25°C (scan rate = 0.2 mV sec^{-1})

Electrode	Tafel slope /mV $decade^{-1}$	Order(p) at E = 650 mV	j/ mA cm^{-2} at η_{O_2}/mV		η_{O_2} /mV at j/ mA cm^{-2}	
			350 mV	400 mV	100	300
$LaCoO_3$	77	0.8	7.2	28.0	467	552
$La_{0.8}Sr_{0.2}CoO_3$	66	1.0	11.9	46.7	436	509
$La_{0.6}Sr_{0.4}CoO_3$	71	1.0	16.3	67.7	417	477
$La_{0.4}Sr_{0.6}CoO_3$	72	1.1	24.1	90.1	406	462
$La_{0.2}Sr_{0.8}CoO_3$	70	1.0	42.4	151.9	383	435

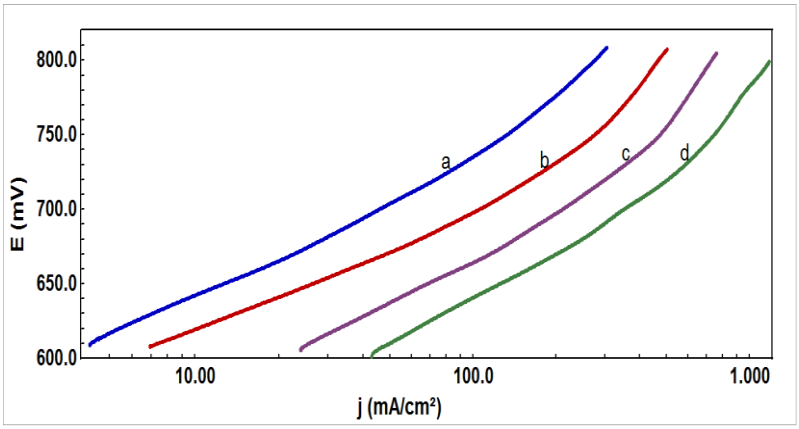

Figure11. Tafel plots for oxygen evolution on the $La_{0.2}Sr_{0.8}CoO_3$ film on Ni at different temperatures in 1 M KOH. a: 20°C b: 30°C c: 40°C d: 50°C

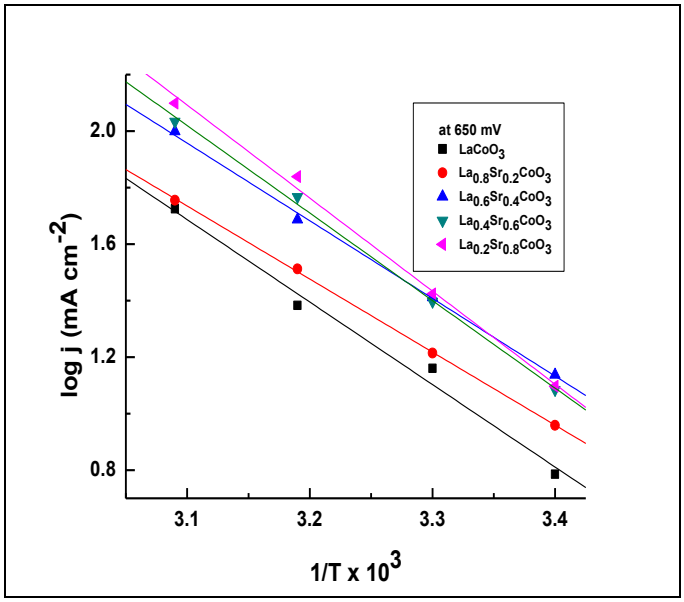

Figure 12. The Arrhenius plot for $La_{1-x}Sr_xCoO_3$ ($0 \leq x \leq 0.8$) film electrode on Ni in 1 M KOH at a constant applied potential (E = 650 mV).

The effect of temperature on oxygen evolution reaction has also been studied with each oxide electrocatalyst. For the purpose, anodic polarization curves were recorded at different temperature in 1 M KOH. A representative polarization curve for $La_{0.2}Sr_{0.8}CoO_3$ is shown in Fig. 11. The current density (j) was estimated from each polarization curve recorded at different temperature and a graph log *j* vs 1/T, as shown in Fig. 12, was plotted at a constant applied potential. Slope of the plot gives the value of standard apparent enthalpy of activation ($\Delta H_{el}^{\circ\#}$). The value of $\Delta H_{el}^{\circ\#}$ was almost similar with each oxide electrode.

The equation $\alpha = 2.303RT/bF$ was used to estimate the transfer coefficient (α) for the OER. Where, R, F and T are the gas constant, Faraday constant and absolute temperature, respectively. The Tafel slope (b) is calculated from the polarization curves obtained at different temperatures. The standard enthalpy of activation ($\Delta H^{\circ\#}$) or standard electrochemical enthalpy of activation was calculated by using the relation, $\Delta H_{el}^{\circ\#} = \Delta H^{\circ\#} - \alpha F\eta$, where, η is the overpotential. The equation [49] given below was used to calculate the $\Delta S^{\circ\#}$ value.

$$\Delta S^{\circ\#} = 2.3R\,[\log j + \Delta H_{el}^{\circ\#}/2.3RT - \log (nF\omega C_{OH^-})]$$

Where, ω (= $k_B T/h$) is the frequency term and $n = 2$, k_B and h are the Boltamann constant and Plank's constant, respectively. The estimated values of transfer coefficient (α), standard apparent enthalpy of activation $\Delta H_{el}^{\circ\#}$, standard enthalpy of activation ($\Delta H^{\circ\#}$) and entropy of activation ($\Delta S^{\circ\#}$) are given in Table 3. The highly negative value of standard entropy of activation ($\Delta S^{\circ\#}$) for OER suggests the role of adsorption phenomenon in the electrochemical formation of oxygen.

Table 3. Thermodynamic Parameters for $La_{1-x}Sr_xCoO_3$ ($0 \le x \le 0.8$) film electrodes at, E = 650 mV

Electrode	α	$\Delta H_{el}^{o\#}$ /kJ mol^{-1}	$\Delta H^{o\#}$ /kJ mol^{-1}	$-\Delta S^{o\#}$ /J deg^{-1} mol^{-1}
$LaCoO_3$	0.76	55.9	81.4	142.2
$La_{0.8}Sr_{0.2}CoO_3$	0.89	49.5	79.3	159.2
$La_{0.6}Sr_{0.4}CoO_3$	0.83	52.6	80.4	146.5
$La_{0.4}Sr_{0.6}CoO_3$	0.81	59.3	86.6	120.6
$La_{0.2}Sr_{0.8}CoO_3$	0.84	63.0	91.2	103.5

4. CONCLUSION

The X-ray diffraction study indicated the formation of pure perovskite phase of the material with hexagonal crystal geometry. The substitution of Sr for La in the base strongly increased the electrocatalytic activity of the oxide and the value being highest with 0.8 mol Sr-substitution. The activity of this oxide is almost six times higher than that observed by $LaCoO_3$. However, thermodynamic parameters are almost unaffected by the Sr-substitutions.

ACKNOWLEDGEMENTS
Authors are thankful to Department of Science and Technology (DST), New Delhi for financial support as Fast Track Scheme for Young Scientist (No.: SR/FT/CS–044/2009).

References

1. S. Trasatti, in The Electrochemistry of Novel Materials, ed. J. Lipkowaski and Philip N. Ross, VCH Weinheim, 1994, p. 207.
2. E. J. M. O'Sullivan and E. J. Calvo, In Electrode Kinetic Reaction, ed. R. G. Compton, Elsecier, Amsterdam, 1987.
3. S. Trasatti and G. Lodhi., In Electrodes of Conductive Metallic Oxides, Part B, ed. S. Trasatti, Elsevier, Amsterdam, 1981.
4. L.G. Tejuca, J. L. F. Feierro and J. M. Tascon, Advances in Catalysis, Vol. 36, Academic Press, New York, 1991.
5. A. K. Ladovos and P. Pomonis, *J. Chem. Soc. Faraday Trans*., 87 (1991) 3291-3297.
6. J. O. M. Bockris and T. Otagawa, *J. Electrochem. Soc*. 131 (1984) 290-302.
7. J. Balej, *Int. J. Hydrogen Energy*, 10 (1985) 89-99
8. A. G.C. Kobussen, F. R. van Buren, T. G. M van Den Belt and H. J. A van Wees, *J. Electroanal Chem.*, 96 (1979) 123-125.
9. Y. Matsumotp, H. Manabe and E. Sato, *J. Electrochem Soc*. 123 (1980) 811-814.
10. H. Wendt and V. Plzak, *Electrochim .Acta* 28 (183) 27-34.
11. G. Fiori and C. M. Mari, *Int. J. Hydrogen Energy*, 7 (1982) 489-493.
12. Y. Terayoka, H. kakebayashi, I. Moriguchi and S. Kagawa, *Chem. Lett*., (1991) 637-676.
13. K. Vidyasagar, J. Gopalkrishanan and C. N. R. Rao, *J. Solid State Chem*., 58 (1985) 29-37.
14. H. Taguchi, D. Matsuda and M. Nagao, *J. Am.. Ceram. Soc*., 76 (1992) 201
15. S. P. Sharibaa, P. J. Pomonis and A. J. Sdoukos, *J. Mater. Chem*., 1 (1991) 781-
16. J. K. Vassiliou, M. Hornbostel, R. Ziebarth and F. J. Disalvo, *J. Solid State Chemistry*, 81 (1989) 208-216.
17. S. K. Tiwari, P. Chartier and R. N. Singh, *J. Electrochem. Soc*., 142 (1995) 148-153.
18. A. N. Jain, S. K. Tiwari, R. N. Singh and P. Chartier, *J. Chem. Soc. Faraday Trans*., 91 (1995) 1871-1875.
19. R. N. Singh, A. N. Jain, S. K. Tiwari, G. Poillerat and P. Chartier, *J. Appl. Electrochem*., 25 (1995) 1133-1138.
20. R. N. Singh, S. K. Tiwari, S. P. Singh, A. N. Jain and N. K. Singh, *Int. J. Hydrogen Energy*, 22 (1997) 557-562.
21. S. K. Tiwari, J. F Koenig, G. Poillerat, P. Chartier and R. N. Singh, *J. Appl. Electrochem*., 28 (1998) 114-119.
22. R. N. Singh, S. K. Tiwari, S. P. Singh, N. K. Singh, G. Poillerat and P. Chartier, *J. Chem. Soc. Faraday Trans*. 92 (1996) 2593-2598.
23. A. N. Jain, S. K. Tiwari and R. N. Singh, *Ind. J. Chem*., 37A (1998) 125-129.
24. N. K. Singh, S.K. Tiwari, and R. N. Singh, *Int. J. hydrogen Energy*, 23 (1998) 775-780.
25. T. Sharma, N. K. Singh, S.K. Tiwari, and R. N. Singh, *Ind. J. Eng. Mat. Sci*. 5 (1998) 38-42.
26. N. K. Singh, B. Lal and R. N. Singh, *Int. J. hydrogen Energy*, 27 (2002) 885-893.
27. R. N. Singh, S. K. Tiwari, T. Sharma, P. Chartier and J. F. Koenig, *J. New Mat. Electrochem. Syst*., 2(1999) 65-69.
28. B. Lal, M. K. Raghunanda, M. Gupta and R. N. Singh, *Int. J. Hydrogen Energy*30 (2005) 723-729.
29. E. M. Gracia, H. A. Taroco, T. Matencio, R. Z. Domingues and J. A.F. dos Santos, *Int. J. Hydrogen Energy*, 37 (2012) 6400-6406.
30. C. Jin, X. Cao, F. Lu, Z. Yang and R. Yang, *Int. J. Hydrogen Energy*, 38 (2013) 10389-10393.
31. C. Jin, X. Cao, L. Zhang, C. Zhang and R. Yang, *J. Power Sources*, 241 (2013) 225-230.
32. P. H. Benhangi, A. Alfantazi and E. Gyenge, *Electrochim Acta*, 123 (2014) 42-50.
33. R. Liu, F. Liang, W. Zhou, Y. Yang and Z. Zhu, *Nano Energy*, 12 (2015) 115-122.
34. C. F. Chen, G. King, R. M. Dickerson, P. A. Papin, S. Gupta, W. R. Kellogg and G. Wu, *Nano Energy*, 13 (2015) 423-432.

35. C. Su, W. Wang, y. Chen, G. yang X. Xu, M. O. Tade and Z. Shao, *Appl. Mater. Interface*, 7 (2015) 17663-17670.
36. X. Cheng, E. Fabbri, M. Nachtegaal, I. E. Castelli, M. El Kazzi, R. Haumont, N. Marzari and T. J. Schmidt, *Chem. Mater*, 27 (2015) 7662-7672.
37. S. Mulkhandi, P. Trinh, A. K. Manohar, A. manivannan, M. Balasubramanian, G. K. Surya Prakash and S. R. Narayanan, *J. Phys. Chem.*, C 119 (2015) 8004-8013.
38. M. Abreu-Sepulveda, P. Trinh, S. Malkhandi, S. R. Narayanan, J. Jorne, D. J. Quesnel, J. A. Postonr Jr and A. Manivannan, *Electrochim Acta*, 180 (2015) 401-408.
39. J. G. Lee, J. Hawang, H. J. Hwang, O. S. Jeon, J. Jang, O. Kwon, Y. Lee, B. Han and Y-G Shul, *J. Am. Chem. Soc*., 138 (2016) 3541-3547.
40. K. Elumeeva, J. Masa, J. Sierau, F. Tietz, M. Muhler and W. Schuhmann, *Electrochmim Acta*, 208 (2016) 25-32.
41. S. Egelund, M. Caspersen, A. Nikiforov and P. Moller, *Int. J. Hydrogen Energy*, 41 (2016) 10152-10160.
42. Y. Zu, W. Zhou, J. Yu, Y. Chen, M. Liu and Z. Shao, *Chem. Mater*, 28 (2016) 1691-1697.
43. R. N. Singh, J. P. Pandey, N. K. Singh, B. Lal, P. Chartier and J. F. Koenig, *Electrochim. Acta*, 45 (2000)1911-1919.
44. N. Fradette and B. Marsan, *J. Electrochem. Soc*., 145 (1998) 2320-2327.
45. PH. Vermeiren, , R. Leysen, H. W. King, G. J. Murphy, and H. Vandenborre, *Int. J. Hydrogen Energy*, 12 (1987) 469-472.
46. R. N. Singh, J. P. Pandey and K. L. Anitha, *Int. J. Hydrogen Energy*, 18 (1993) 467-473.
47. Trasatti S, in Electrochemical Hydrogen Technology, ed. Wendt H, Elsevier, Amsterdam, 1990, p. 104.
48. S. P. Singh, R. N. Singh, P. Chartier and G. Poillerat, *Int. J. Hydrogen Energy*, 20 (1995), 203-210.
49. E. Gileadi, *Electrode Kinetics*, (VCH Publishers Inc., New York), 1993 p.151